Development and test of a multi-rotor plant protection drone for narrow spraying applications

Chuyi Wang[1], Qingxuan Kong[1], Jinge Han[2], Xin Han[1,3*], Yubin Lan[1*], Guobin Wang[1,3], Yingkuan Wang[4], Maochang Song[1], Xinyue Gou[1]

(1. *College of Agricultural Engineering and Food Science, Shandong University of Technology, Zibo 255000, Shandong, China*;
2. *School of Binzhou Polytechnic, Binzhou 256603, Shandong, China*;
3. *Institute of Modern Agricultural Equipment, Shandong University of Technology, Zibo 255000, Shandong, China*;
4. *Academy of Agricultural Planning and Engineering, Ministry of Agriculture and Rural Affairs, Beijing 100125, China*)

Abstract: Unmanned aerial vehicle (UAV) wind field airflow is the main factor affecting spraying width and operational effect. Under the soybean and maize compound planting mode, the width of the spray droplets of UAV aerial spraying is easily sprayed on other crops around the target crop by mistake due to the influence of the wind field. In order to solve this problem, a narrow-width spraying UAV equipped with an airflow guidance device was developed in this study, which can achieve precise spraying on target crops within a narrow operation width and reduce the impact of droplet drift on surrounding non-target crops. The wind field of the flight platform was simulated via simulation software, and the wind field distribution characteristics corresponding to three sizes of the guidance device were analyzed. It was verified that the guidance device has a segmentation effect on the wind field, and the optimal size of the guidance device was determined as 0.92 m accordingly. Meanwhile, the installation position and quantity of nozzles were determined to be set at the position with the minimum airflow disturbance. The wind speed at measuring points with different angles on four diameters at five heights under the UAV hovering state was tested through bench tests, to further verify the simulation results and appropriately adjust the nozzle position according to the measured wind speed. Outdoor flight spraying tests were carried out, and the results showed that when the 0.92 m guidance device was applied at a flight altitude of 1.00 m, the effective spray width was only 1.46 m according to the droplet deposition density on the coated paper of three test collection belts. Under the maize-soybean composite planting pattern, the field spraying test yielded results of 18.0%-30.0% deposition rate in the maize area and 0.1%-1.6% in the soybean area with maize as the operational target. A predictive effect of wind field simulation on the installation position of nozzles where droplets suffer the least wind field disturbance under aerial spraying conditions was confirmed. The UAV wind field can be effectively segmented by the airflow guidance device, and the diameter of the droplet-laden airflow column can be reduced, thus realizing narrow-width spraying.

Keywords: narrow spraying, plant protection drone, downwash wind field guidance, CFD
DOI: 10.25165/j.ijabe.20261902.9472

Citation: Wang C Y, Kong Q X, Han J G, Han X, Lan Y B, Wang G B, et al. Development and test of a multi-rotor plant protection drone for narrow spraying applications. Int J Agric & Biol Eng, 2026; 19(2): 1–12.

1 Introduction

With the development of agricultural technology, reducing labor intensity and improving operational efficiency are the general trends of agricultural development. Complete mechanization is the key way to solve this problem, but it is difficult for the traditional ground machinery to meet the special agronomic requirements of maize and soybean composite planting, especially because maize and soybeans cannot be used with the same herbicides for plant protection operations. To address this chanllenge, narrow spraying technology has emerged as a promising solution, with critical implication for targeted pesticide application in complex intercropping systems. Narrow spraying, as a new pest control technology, provides a new way to effectively reduce pesticide use[1]. The technology minimizes pesticide loss by precisely controlling the spraying range and spraying volume, thus enhancing the efficiency of pesticide use. The application of narrow spraying technology is of strategic significance for reducing environmental pollution, ensuring the quality and safety of agricultural products and the sustainable development of China's agricultural production, and is expected to play an important role in future agricultural production practices.

In order to solve the difficulty of accurately spraying the target area in mixed planting, Zhang et al.[2] designed a highland gap spray

Received date: 2024-10-29 **Accepted date:** 2025-11-19

Biographies: Chuyi Wang, MS candidate, research interest: aviation plant protection technology and equipment, Email: 13098455464@163.com; **Qingxuan Kong**, MS candidate, research interest: agricultural pest and disease control technology, Email: 3280318641@qq.com; **Jinge Han**, MS candidate, research interest: plant protection UAV technology and application, Email: 17852033561@163.com; **Guobin Wang**, PhD, Associate Professor, research interest: aviation plant protection technology, Email: guobinwang@sdut.edu.cn; **Yingkuan Wang**, PhD, Professor, research interest: smart agriculture technology, Email: wangyingkuan@163.com; **Maochang Song**, MS candidate, research interest: agricultural pest and disease control technology, Email: 18866738491@163.com; **Xinyue Gou**, MS candidate, research interest: field management technology and equipment, Email: 13581011853@163.com.

***Corresponding author: Xin Han**, PhD, Professor, research interest: aviation plant protection technology and equipment. School of Agricultural and Food Science, Shandong University of Technology, Zibo 255000, Shandong, China. Tel: +86-15953359191, Email: hanxin_1979@163.com; **Yubin Lan**, Professor, Dean, research interest: aviation plant protection technology and equipment. School of Agricultural and Food Science, Shandong University of Technology, Zibo 255000, Shandong, China. Email: ylan@sdut.edu.cn.

bar sprayer with a spray width of 8 m. The sprayer has a wind screen-assisted spraying system that can reduce the droplet drift and the airflow interference. However, this way of spraying cannot be applied simultaneously on maize and soybeans. However, this system cannot achieve differential and simultaneous spraying for maize and soybean strips, failing to meet the specialized agronomic needs of pesticide application in maize-soybean intercropping. Targeted at this limitation, related research has proposed multi-row spraying system with isolation baffles to adapt to intercropping spraying scenarios. A folding waist steering chassis was adopted to ensure the rapid and convenient movement of the machinery in the field. It also adopts a height-adjustable spraying bar to realize the simultaneous spraying of plants at different heights, as well as an auxiliary airflow to quickly atomize the medicine liquid, which improves the utilization rate of the pesticide. Shang et al.[3] designed a small electric self-propelled sprayer. The system includes a soybean medicine box, maize medicine box, double diaphragm pumps, liquid pipeline, anti-drift nozzle, etc. In the spraying process, maize, soybeans, and different pesticides were processed by the diaphragm pumps into the corresponding pipeline system, through the multi-channel control valves, then through the spray nozzle atomization deposited in the foliage. To achieve the band directional application of medication, in order to prevent the liquid from drifting, between different planting zones with a partition plate, to avoid the drift of liquid, in order to avoid the drift of liquid. The self-balancing precision drug application and fertilization plant protection machine developed by Wang et al.[4] can realize the self-balancing adjustment of the integrated spray bar. However, the soybean is a high and low crop, and the amount of the required drug and the position of the spraying and so on are all different, so that the machine cannot realize split- belt targeted spraying. Cheng[5] developed a self-propelled upland gap spray bar belt spraying machine, retrofitted with two sets of spraying systems. It can be applied synchronously on maize and soybean, but since it is fuel-driven it cannot meet the energy-saving low-carbon environmental protection needs.

In recent years, aerial plant protection technology has developed rapidly. The advantages of multi-rotor plant protection UAVs in agricultural plant protection are mainly manifested in two core dimensions: on one hand, they have faster operating speed and wider coverage, which can significantly improve the efficiency of field plant protection operations[6,7]; on the other hand, they can achieve higher operating precision and controllable droplet deposition through the regulation of spray parameters and rotor downwash airflow[8,9].

However, the UAV wind field determines the spray range, and the spray amplitude produced by the UAV spray range is determined by the volume of airflow[10]. Each rotor of the multi-rotor UAV is rotating at high speed, which will give the air a downward force, and a large amount of air is continuously pushed downward, converging into an airflow with objective downward movement of intensity, which is the downward pressure wind field of the UAV[11]. Additionally, the maximum spraying range of commercially available UAV can be up to 4 m. It is more difficult to spray a single crop in a mixed cropping pattern, and it is easy to spray out of other non-target areas[12]. Spraying out of the target area may cause serious damage to neighboring crops and injury to the spraying operator. Especially when spraying herbicides, spray heights in the range of 1-4 m above the surface of the crop canopy are prone to potential drift, and drug damage to sensitive crops in the vicinity of the sprayed area can be a great challenge[13]. The implementation of droplet drift risk assessment and droplet drift reduction techniques based on field measurements is an important aspect in the development of UAV application technology[14,15].

Since the wind field of the UAV determines the spraying range[16], in this study, the airflow in the downwash wind field under the UAV rotor was simulated via computational fluid dynamics (CFD), to investigate the effect of the downwash wind field guidance device on wind field segmentation. This method has the advantages of lower cost and higher efficiency compared with field tests, and has been widely adopted by UAV researchers with the rapid development of CFD technology[17]. In the field of aerial spraying droplets to simulate the effect of wind field changes on the spraying effect of this method, wind tunnel tests and other methods can also be applied to simulate the effect of wind field changes on spraying performance, but such experimental resources are not widely available in universities. In the field of CFD, ANSYS-Fluent is one of the most mature solid-fluid coupling simulation softwares. Yao et al.[18] used ANSYS software for CFD to simulate the flow field distribution of a quadcopter UAV under the influence of wind disturbance to investigate the effect of wind disturbance on the aerodynamic performance of quadcopter UAV with different rotor arrangements[19]. Wang et al.[20] used the CFD method for the numerical simulation of the air flow field. They established a real-time method based on inverse distance weighting (IDW) to calculate the droplet deposition distribution of a six-rotor plant protection UAV, and the relative error between the tested and simulated values of the method was within 12%[21]. Li et al.[22] summarized the droplet drift and deposition patterns, vortex effects, and rotor-induced downwash airflow through a series of CFD simulations using a discrete phase model (CFD) to simulate the motion of droplet particles. They proposed two methods to reduce droplet drift. This study not only analyzed the way downwash airflow affects droplet motion, but also verified the accuracy of the simulation analysis through field tests.

Currently, the mainstream compound planting and drug application machinery on the market is ground machinery. Ground machinery may crush plants in the process of traveling, especially for high stem crops like maize. The use of ground machinery to apply medicine may increase the risk of damage to plants, while the drone in the air when applying medicine is able to avoid the plants to spray medicine directly[12,14], reduce the damage to plants, and add isolation boards or wind curtains and other physical isolation methods between the maize belt and the soybean belt. Additionally, the planting drone downward-pressure wind field is similar to the wind screen device in that, after adding a reasonable down pressure wind field guide device, it can make the down pressure wind field quickly float the liquid to the ground to reduce the drift.

To address these persistent chanllenges in precision spraying for maize-soybean strip intercropping, this work proposes and develops a novel multi-rotor plant protection UAV equipped with a segmented airflow guidance system, which enables narrow-width spraying and effectively mitigates off-target droplet drift. By installing a downwash wind field guidance device on the UAV, the conical downward pressure wind field diffused by the UAV is converged into a more concentrated, stronger and more regular-shaped wind field, which reduces the drift of the chemical liquid in the air and ensures that the chemical droplets are sprayed more accurately and intensely in a narrow range to act on the target crops. This avoids waste caused by the spread of droplets between rows, making it suitable for precise spraying operations of narrow row spacing crops, and improving the accuracy and efficiency of spraying. This improvement not only significantly increases the utilization rate of the pesticide, but also reduces accidental spraying of the surrounding non-target crops, thus significantly increasing the overall spraying efficiency and precision. In this way, plant protection drones are able to achieve more efficient and precise pesticide application when performing plant protection tasks, which is of great significance in enhancing agricultural production efficiency and crop protection.

2 Overall structure and working principle of the narrow-spraying UAV system

2.1 Overall composition of the drone

The overall planning and design of the multi-rotor plant protection UAV suitable for narrow spraying includes the UAV flight platform design requirements, the design requirements of the downward-pressure wind field guidance device, the total mass estimation, the design of the spraying device, and the selection of the power system. The whole aircraft composition diagram is shown in Figure 1.

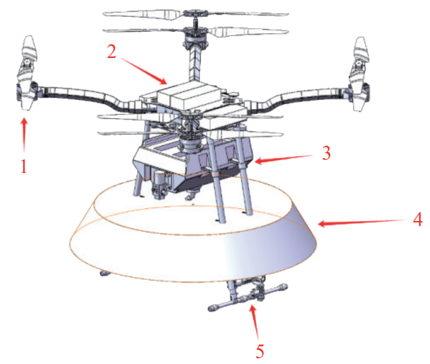

1. Power system 2. Power supply system and flight control system 3. Medicine box and water pump 4. Guide cover 5. Nozzle

Figure 1 Layout design of the UAV

2.2 Working principle of the narrow-spraying system

During the operation of the plant protection UAV, the flight altitude and operation trajectory are precisely controlled by the flight control system, and the downwash airflow field is generated by the high-speed rotation of the rotors. The rotor downwash airflow field of the conventional plant protection UAV presents a conical diffusion distribution, which easily causes lateral droplet drift and fuzzy boundary of the effective spray width, result in an inability to achieve narrow-band targeted pesticide delivery with clear spray boundaries. For this reason, the narrow-width spraying UAV developed in this study is fitted with a dedicated airflow guidance device, which reshapes the conical diffused downwash airflow from the rotors into a collimated, vertically oriented directional airflow, and constrains the lateral spread of droplet-carrying airflow during its doenward movement.

During the spraying operation, the pesticide liquid is delivered to the nozzles by a pressure pump and atomized into droplets for ejection. The nozzles are arranged in the low-speed airflow area on both sides of the airflow guidance device. The airflow in this area has weak disturbance and stable flow field, which can greatly reduce the interference of downwash airflow on the initial movement of droplets and facilitate their vertical deposition. A high-speed downwash airflow area is formed outside the airflow guidance device, which acts as a wind field barrier with a clear boundary, restricts the escaped droplets to settle rapidly to the target operation area, and further suppresses lateral drift.

The effective spray width can be flexibly and precisely adjusted through the coupling of flight operation parameters and the structural parameters of the airflow guidance device. When operating along the target crop roes in a maize-soybean strip intercropping system, this device confines the droplet-laden airfloe strictly within the target operation zone, drastically loweringf the risk of pesticide drift to adjacent non-target crop rows, and enabling row-specific directional precision pesticide application for different crop strips.

2.3 Design of the downwash wind field guidance device

In terms of the design of the down-pressure wind field guidance device, it is important to consider the impact of the down-pressure wind field guidance device on the performance of the plant protection UAV and its effect on air infusion. The UAV generates lift through its rotor blades. When the rotors rotate rapidly, they push the air downward, creating upward lift according to Newton's third law (action and reaction). This lift allows the UAV to overcome gravity and achieve lift off. When the downwash wind field guidance device is located below the plant protection UAV, it will increase the air resistance of the UAV, and the increased resistance will result in the UAV's power system needing to provide more power to maintain the same flight speed and altitude, thus affecting the battery life. Therefore, the selection of an approximate streamlined downdraft wind field guide can reduce the drag, but considering the cost of fabrication and transportation, the downdraft wind field guide was designed in the shape of a convex platform with the angle of the upper bottom edge being 120°.

In order to compare the relationship between different downdraft wind field guides, a total of three kinds of downdraft wind field guides were designed according to their dimensions. The three sizes of lower diameter are 800 mm, 920 mm, and 1040 mm, respectively, as shown in Figure 2.

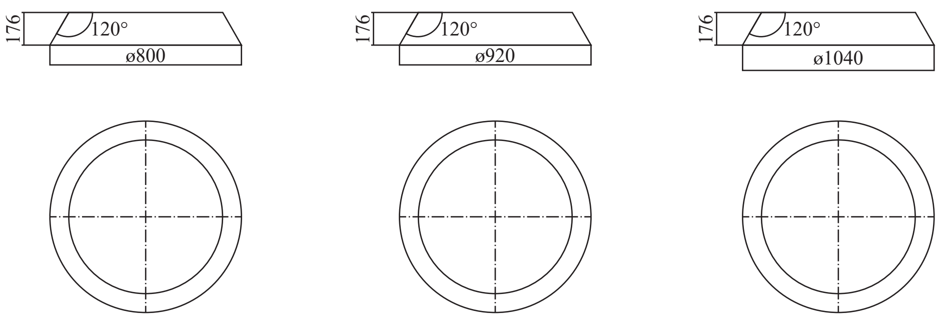

a. Modeling of 800 mm diameter downdraft wind field guides
b. Modeling of 920 mm diameter downdraft wind field guides
c. Modeling of 1040 mm diameter downdraft wind field guides

Figure 2 Plant protection UAV downward pressure wind field guidance device (mm)

3 CFD simulation of the UAV downwash wind field

3.1 Physical structure modeling and processing

To simulate the airflow in the wind field under the rotor of a UAV, the accuracy of the blade model determines the accuracy of the simulation results[22]. The shape of the blade is curved and complex, and it is difficult to build it directly with the drawing software. Therefore, the profile of the blade was scanned by a HandyScan 700 handheld 3D scanner (the physical image of the blade is shown in Figure 3a), and post-processing was carried out via Geomagic Design X software to realize the inverse modeling of the 3D surface of the rotor blade. The scanned 3D model of the rotor blade is shown in Figure 3b.

During the simulation, the airflow is mainly generated by the high-speed rotation of the rotor blades, and other components of the UAV have negligible influence on the flow field simulation. To simulate the real operation state of the UAV, 3D modeling of the whole UAV was carried out. Due to the complex shape of the plant protection UAV, additional unnecessary work will be added when meshing, so it was necessary to simplify its processing, with the specific processing as follows: 1) the holes in the parts were filled and chamfers and rounded corners were removed; 2) the electronic equipment and batteries inside the UAV were removed, and the pesticide tank was simplified into a simple rectangular body; 3) some of the landing frames of the UAV were deleted; 4) the spraying system of the UAV was removed. The simplified UAV model was meshed into the external flow field and rotation domain, and the results of the meshing are shown in Figures 3e and 3f.

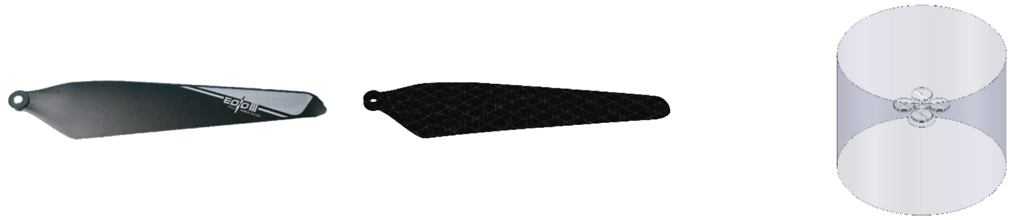

a. Paddle physical picture b. Paddle three-dimensional drawing c. External flow field

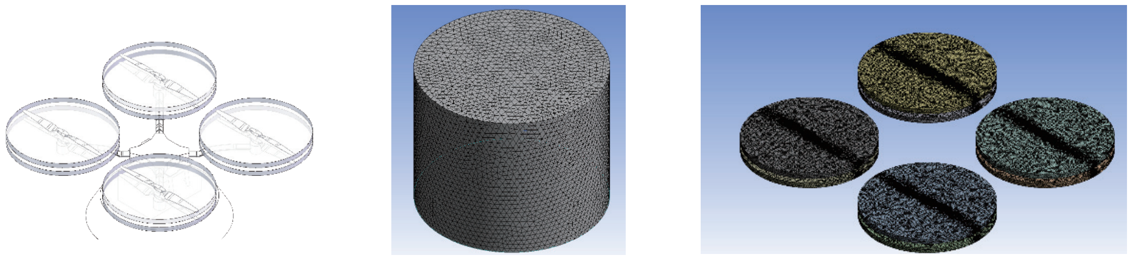

d. Rotating area e. External flow field meshing f. Rotation domain meshing

Figure 3 Modeling and simplification of key UAV components

3.2 Simulation environment and parameter setting

According to the field operation parameters of the multi-rotor plant protection UAV, when the CFD method was applied for simulation and solution of the UAV, the simulation environment under the hovering state of the UAV was established, and the relevant boundary conditions and solution parameters were set. The flow field computational domain model was set as a cylinder, which represents the operating environment where the UAV is located. The rotating area where the propeller is located was defined as the dynamic domain mesh. The specific setup process was as follows: the upper end of the fluid domain was set as the inlet and defined as a pressure inlet; the lower end of the fluid domain was set as the outlet and defined as a pressure outlet; the wall of the fluid domain was set as a wall boundary; eight rotational domains were named fan-a1, fan-a2, fan-b1, fan-b2, fan-c1, fan-c2, fan-d1, and fan-d2 respectively, and the corresponding rotation direction was set for each blade; the slip mesh model was adopted for the rotational domains, and the coordinate origin was input according to the coordinates used in the modeling process; since the rotational speed during hovering was 2351 r/min, the rotational speed was set to 2351 r/min, and the direction of the rotational axis (y-axis) was set to –1 according to the right-hand rule; and the Semi-Implicit Method for Pressure-Linked Equations-Consistent (SIMPLEC) algorithm was adopted for the pressure-velocity coupling scheme. The total number of time steps was set to 100, the single time step was set to 0.05 s, and the number of iterations per time step was set to 25. The built simulation environment is shown in Figure 4.

As the down-pressure wind field guide device is mounted on the UAV platform, its size has relatively strict requirements. A large size will lead to a heavy weight, which will reduce the UAV endurance. In summary, to clarify the influence of the device diameter on the distribution law of the UAV wind field, the fixed structural parameters were uniformly adopted as follows: the angle of the upper base and the side of the upper base is 120°, and the height of the device is 176 mm. Given the height of the device, when the diameter of the lower bottom is more than 110 mm, it will block most of the rotor wind field, resulting in a significant decrease in the range of the UAV. When the diameter of the lower bottom is lower than 800 mm, the blockage of the wind field is small, and the effect on the wind field is very small. Thus, the lower bottom diameters selected in this study were set to 800 mm, 920 mm, and 1040 mm. The downward-pressure wind-field guidance device modeling is shown in Figure 5.

3.3 Simulation model results and analysis

In this section, the plant protection UAV equipped with down-pressure wind field guidance devices with diameters of 0.80 m, 0.92 m, and 1.04 m under hovering state with a rotor speed of 2351 r/min was taken as the research object, and convergent data were finally obtained after thousands of iterations. In order to deeply explore the distribution characteristics of the down-pressure wind field generated by the rotor in the horizontal and vertical directions, the velocity section of the wind field in the height range of 0.42-0.74 m was obtained. In addition, a 3D coordinate system was established with the point below the UAV center point set as the zero point, and five wind speed sections of the wind field were set in the vertical direction (h_1=0.42 m, h_2=0.50 m, h_3=0.58 m, h_4=0.66 m, h_5=0.74 m). The detailed analysis results are shown below.

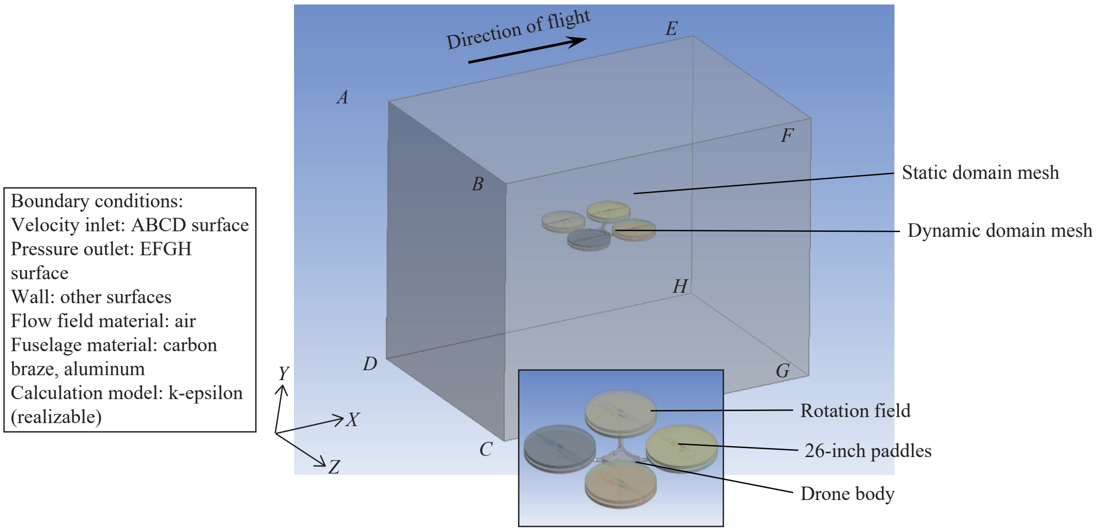

Figure 4 Simulation environment construction

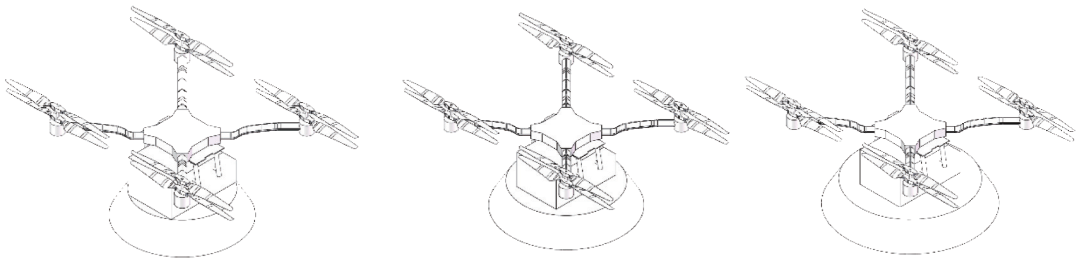

a. Modeling of 800 mm diameter downdraft windfield guide b. Modeling of 920 mm diameter downdraft windfield guide c. Modeling of 1040 mm diameter downdraft windfield guide

Figure 5 Modeling of the whole machine with different sizes of airflow guides

To investigate the downwash airflow field and the vertical distribution velocity nephograms of the plant protection UAV equipped with 0.80 m, 0.92 m, and 1.04 m downwash airflow field guidance devices, the velocity nephograms at different height interfaces (Figure 6) and the velocity nephograms at the main view plane of the rotor (Figure 7) were analyzed based on the simulation results.

1) The velocity vector distribution of the downwash airflow field in the *XOZ* plane was presented by the simulation results shown in Figure 6. Combined with the velocity nephograms at five sections with different heights, the distribution law of the downwash airflow field of the UAV equipped with guidance devices with diameters of 0.80 m, 0.92 m, and 1.04 m was obtained. The distribution characteristics of the downwash airflow field were summarized according to the morphology of the velocity nephograms as follows: The downwash wind field was blocked by the downwash wind field guidance device, and the center of the downwash wind field guidance device is divided into the center of the circle. The speed presents a step shape, from inside to outside, and the speed increases first and then decreases.

2) In the place not covered by the down-pressure wind field guidance device, the velocity was distributed in a stepped pattern with the rotor center as the circle center, the speed was in a stepped shape, and the speed gradually decreases from inside to outside.

3) From 0.42 to 0.74 m, the shielding range of the downwash wind field guidance device gradually decreases, and the speed ladder distribution gradually becomes less obvious.

4) The maximum wind speed in the downforce wind field of the rotor appears at the center of the rotor, and the velocity at the corresponding position decreases with the increase of the distance from the rotor.

5) For the 0.80 m downwash airflow field guidance device, the low-speed area was within the range of 0.42-0.50 m below the device with an obvious boundary, and the wind field inside the guidance device in the area below 0.50 m was gradually affected by the rotor. For the 0.92 m guidance device, the low-speed area had a clear boundary within 0.42-0.58 m below the device, and the wind field inside the device in the area below 0.58 m was gradually but significantly affected by the rotor. For the 1.04 m guidance device, the low-speed area was clearly segmented within 0.42-0.66 m below the device, and the wind field inside the device in the area below 0.66 m was gradually but significantly affected by the rotor. It was concluded that the vertical guidance length for the wind field increased with the increase of the diameter of the downwash airflow field guidance device.

6) At the same slice height, the larger the diameter of the downwash wind field guidance device, the larger the influence range on the downwash wind field.

As the four rotors rotated in different directions, the air was cut and disturbed, and an air pressure difference effect was generated. The airflow near the rotors was guided to the rotor wind field, forming a mutually disturbed airflow field, and the obvious low-

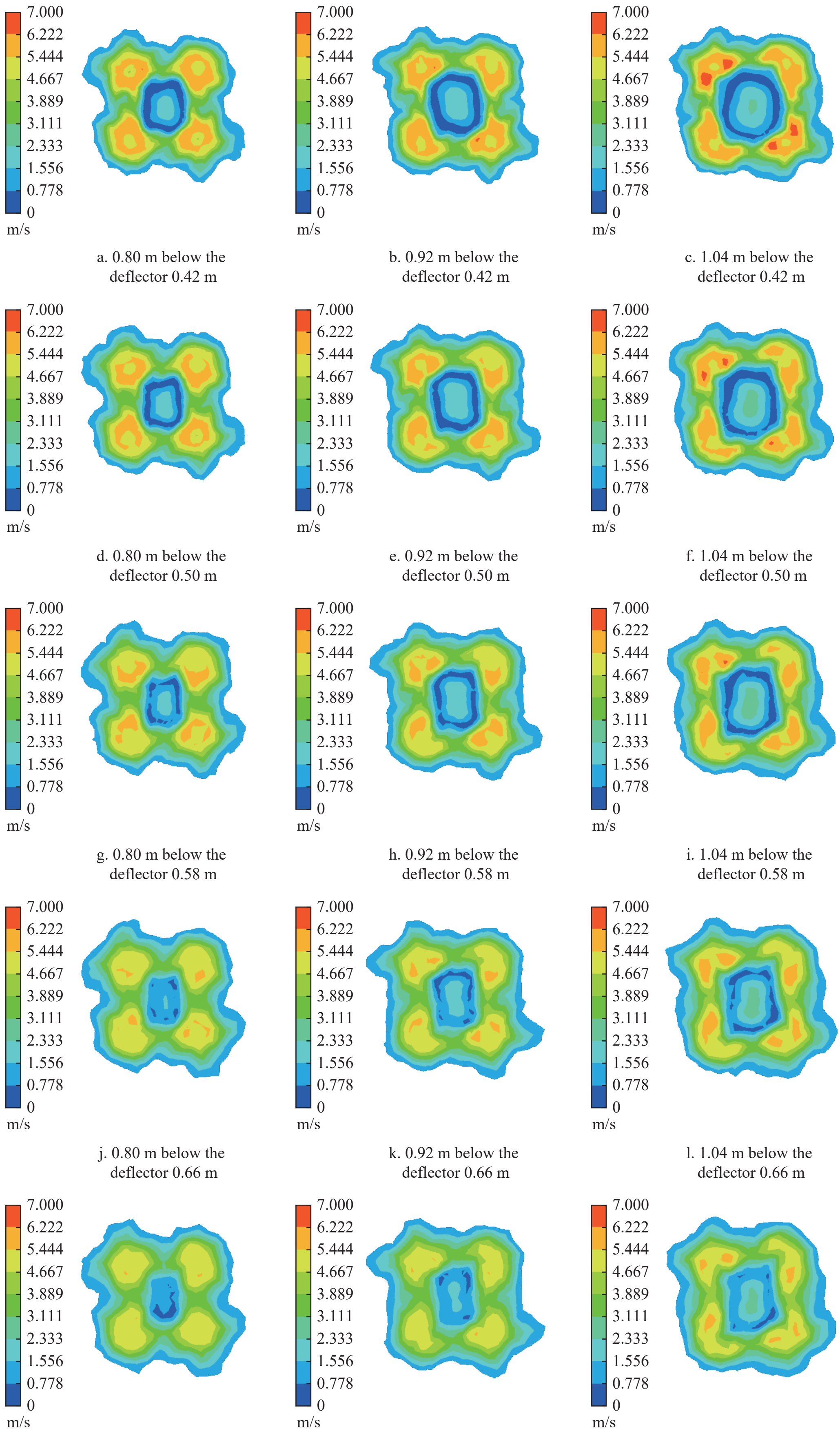

a. 0.80 m below the deflector 0.42 m
b. 0.92 m below the deflector 0.42 m
c. 1.04 m below the deflector 0.42 m
d. 0.80 m below the deflector 0.50 m
e. 0.92 m below the deflector 0.50 m
f. 1.04 m below the deflector 0.50 m
g. 0.80 m below the deflector 0.58 m
h. 0.92 m below the deflector 0.58 m
i. 1.04 m below the deflector 0.58 m
j. 0.80 m below the deflector 0.66 m
k. 0.92 m below the deflector 0.66 m
l. 1.04 m below the deflector 0.66 m
m. 0.80 m below the deflector 0.74 m
n. 0.92 m below the deflector 0.74 m
o. 1.04 m below the deflector 0.74 m

Figure 6 Cross-sectional diagram of the velocity of the UAV downward pressure wind field at different altitudes

speed area was segmented by the downwash airflow field guidance device. To clarify the movement law and distribution characteristics of the airflow in the wind field below the UAV equipped with guidance devices of different sizes, the velocity nephograms of the longitudinal section of the UAV with guidance devices of 0.80 m, 0.92 m, and 1.04 m are drawn based on the simulation results as shown in Figure 7.

The distribution of the velocity nephogram of the UAV in the longitudinal section is presented in Figure 7, and the following conclusions were obtained: 1) The downwash airflow field was symmetrically distributed with the rotor as the symmetry center, which was generated by the pressure difference induced by the high-speed rotation of the rotor airfoil; 2) It was observed from Figures 7a-7c that the internal vortex intensity increased significantly with the increase of the diameter of the downwash airflow field guidance device, while the distance between the upper boundary of the vortex and the bottom of the guidance device had no significant difference; 3) A low-speed zone with a certain range was formed below the downwash airflow field guidance device. When nozzles were arranged in this zone, the interference of the downwash airflow field on the sprayed droplets could be effectively avoided, and the droplet drift could be significantly reduced; 4) An obvious boundary was formed between the low-speed zone below the downwash airflow field guidance device and the high-speed zone of the airflow field generated by the UAV rotor blades. The droplets escaping from the low-speed zone could be quickly deposited to the ground under the action of the high-speed airflow, thus avoiding droplet drift to the adjacent crops and the resulting phytotoxicity risk; 5) It was observed from the figure that the low-speed zones on both sides of the downwash airflow field guidance device were symmetrically distributed about the center line of the guidance device. Two nozzles could be arranged in this symmetric low-speed zone respectively, and the spacing between the nozzles increased with the increase of the size of the guidance device.

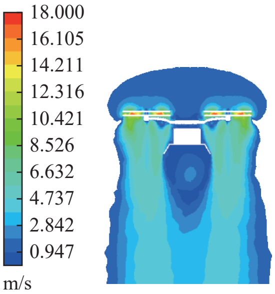

a. Velocity cloud diagram of longitudinal section of 0.80 m air deflector

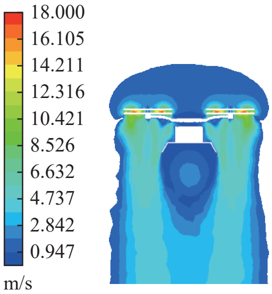

b. Velocity cloud diagram of longitudinal section of 0.92 m air deflector

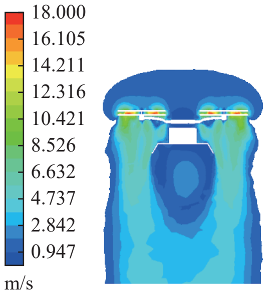

c. Velocity cloud diagram of longitudinal section of 1.04 m air deflector

Figure 7 UAV longitudinal section velocity cloud chart

4 Materials and methods

4.1 Indoor bench test and wind speed measurement of UAV downwash airflow field

To meet the requirements of the UAV downwash wind field measurement test and ensure the accuracy of test data, the support frame below the UAV was minimized to reduce its interference with the wind field. On this basis, the test platform was designed as a door-frame structure, with the UAV fixed directly below the platform. The test schematic diagram is shown in Figure 8. In accordance with the needs and regulations of the UAV field operation, the height of the UAV platform was set to 3 m, and the height of the UAV can be adjusted through the bolt range of 1-3 m. The main material is aluminum profile with low density, strong load-bearing capacity, and reusability. The test platform is supported by four 4040 aluminum profiles. There are support structures on both sides of the aluminum profiles to prevent side-turning, and the four support rods were fixed with “I” type drone connection brackets. In order to ensure the safety of the experiment, the test platform is equipped with a protective net on the periphery. The rotor speed is measured by a laser tachometer below the UAV. To measure the speed of the wind field, the Smart Label GM816 Bluetooth anemometer is used, which can measure the wind speed remotely to ensure the safety of the experiment. The field diagram is shown in Figure 8.

In the previous section, the longitudinal and transverse sections of the fluid simulation of the plant protection UAV were analyzed respectively, and the conclusion that the corresponding nozzle spacing varies with the layout of different downwash airflow field guidance devices was obtained. To further investigate the horizontal and vertical distribution law of the rotor downwash airflow field and the layout scheme of nozzles, the wind field velocity sections within the height range of 0.42-0.74 m were drawn. A 3D coordinate system was established with the point below the UAV center point set as the zero point, and five wind field velocity sections were set in the vertical direction (h_1=0.42 m, h_2=0.50 m, h_3=0.58 m, h_4=0.66 m, h_5=0.74 m). Three adjacent measuring points (r_1, r_2, r_3) on the same radius in the X and Y planes were set as wind speed measuring points at every 60° interval with the zero point as the center of the circle. The layout of each measuring point is shown in Figure 9.

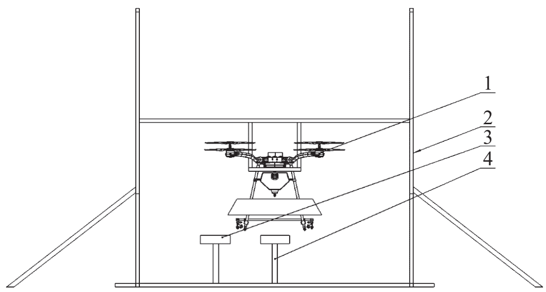

1. Plant protection drone 2. Test bench 3. Tachometer 4. Anemometer

Figure 8 Plant protection drone test bed structure diagram

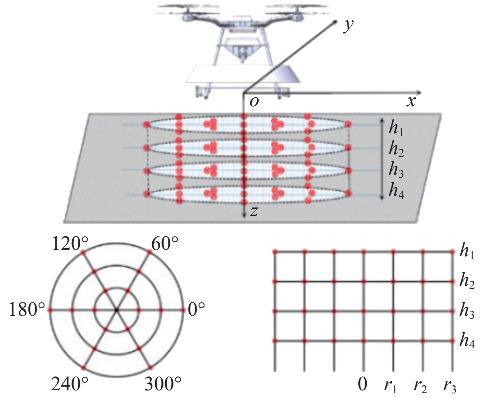

Note: For 0.80 m downwash wind field guide device: r_1=0.17 m, r_2=0.34 m, r_3=0.51 m; For 0.92 m downwash wind field guide device: r_1=0.19 m, r_2=0.38 m, r_3=0.57 m; For 1.04 m downwash wind field guide device: r_1=0.21 m, r_2=0.42 m, r_3=0.63 m.

Figure 9 Measurement point location distribution

4.2 Effective spray width test

The effective spray width of a plant protection UAV is defined as the maximum width of the area that can be effectively covered and treated by the UAV during plant protection operations (e.g., pesticide application and spraying). To verify the optimal spray performance of the optimized guidance device, the subsequent tests were carried out with the downwash airflow field guidance device with an optimal diameter of 0.92 m. In accordance with the Technical Specification for Quality Evaluation of Plant Protection Unmanned Aircraft (NY/T 3213-2018) issued by the Ministry of Agriculture and Rural Affairs of the People's Republic of China, the test layout was designed as shown in Figure 10. Three droplet collection belts were arranged in a flat test site with an interval of 5.00 m between belts. On each collection belt, 13 sampling points were arranged at eauql 0.20 m intervals, and the center flight line was marked as 0. Six collection points were arranged on both left and right sides of the center line, which were marked as –1.20 m, –1.00 m, –0.80 m, –0.60 m, –0.40 m, –0.20 m, 0.20 m, 0.40 m, 0.60 m, 0.80 m, 1.00 m, and 1.20 m in sequence. All sampling points were horizontally mounted on aluminum profile supports at a consistent height of 0.20 m above ground, and the collection cards (coated paper) were horizontally clamped on the brackets. Before the test, 5 g/L of allura red was added into the liquid solution as a spray colorant for the quantitative determination of droplet deposition[23]. The operation height was set as 1.00 m, the flight speed was set as 2.50 m/s, and the spray flow rate was set as 0.52 L/min. Spraying was started 50.00 m before the UAV entered the sampling area, and was stopped 50.00 m after the UAV flew out of the operation area. This operation mode was adopted to ensure the stability, continuity, and full coverage of the spraying process in the sampling area. Each test was repeated for three times to obtain valid effective spray width data, and the average value of the three repeated tests was taken as the final result. After the spraying operation, the collection cards were left to stand until the droplets on the cards were completely dried. Then the collection cards were collected in sequence, and each group of cards was placed in an independent sealed bag for subsequent analysis and evaluation.

4.3 Field spraying test under soybean-maize complex planting pattern

According to the 4:3 model planting pattern given in the "2022 Provincial Soybean and Maize Belt Compound Planting Production Management Technology Preliminary Plan" issued by the Shandong People's Government, the prepared soybean and maize models were arranged according to the soybean row spacing of 0.40 m, maize row spacing of 0.50 m, and the spacing between the soybean belt and maize belt of 0.65 m, as shown in Figure 11.

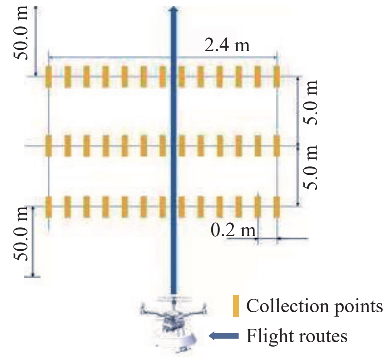

a. Schematic diagram of the test program

b. Effective spray width test site

Figure 10 Effective spray width test experiment

One fog droplet sampling point was placed in the middle of the maize belt and soybean belt, i.e., six spacing sampling points were arranged, and fog droplet sampling points were arranged in the vertical direction along the maize and soybean canopies in the upper, middle, and lower three layers. A total of 33 collection points were arranged, in which the spacing between the upper and middle layers, as well as the middle and lower layers of the maize canopy, was 0.15 m, and the spacing between the upper layer of the soybean and the middle, and the middle and the bottom were both 0.10 m, as shown in Figure 11. For the convenience of statistical analysis, the maize, spacing sampling points, and soybeans were recorded as 1-13 from left to right.

Prior to the test, 5 g/L of allura was added to the solution as a spray stain to determine the amount of spray droplet deposition. The operating height was set at 1 m and the flight speed was 2.5 m/s for the spraying work. The spray flow rate was set at 0.52 L/min, and the operation was started 50.0 m before the sampling area, and the spraying was stopped 50.0 m after flying out of the operation area. Measurement was completed, and after the fog droplets on the collection card dried, the fog droplet collection cards were collected in order and put into a sealed bag by group. The test site is shown in Figure 11.

In accordance with GB17997-2008 Pesticide Spraying Machinery (Apparatus) Field Operation Procedures and Spraying Quality Evaluation and ISO22866:2005 Equipment for Crop Protection—Methods for Field Measurement of Spray Drift, droplet deposition tests were carried out via the deposition percentage method, and the deposition rate was adopted as the index to evaluate the droplet deposition effect of aerial operations. The ratio of the allura red area on the test card to the total area of the test paper after UAV spraying was calculated via computer recognition technology[24]. The allura red on the test card is red, so the red enhancement method is used for grayscaling, followed by image filtering and binarization to define the edges and complete the output of the feature quantity (area ratio)[23].

$$\Phi = \frac{S_1}{S} \times 100\% \tag{1}$$

where, Φ is sedimentation rate, %; S_1 is area in red, cm^2; S is overall test paper area, cm^2.

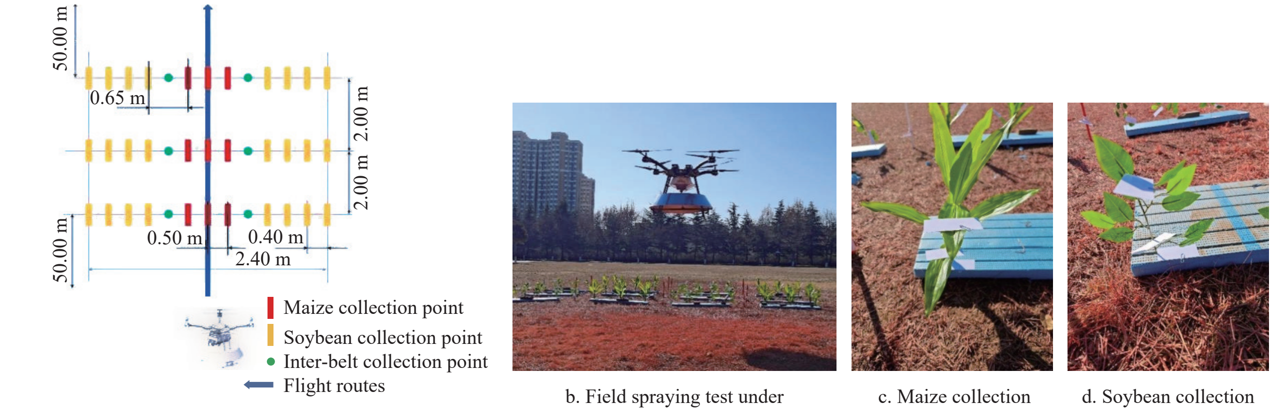

a. Schematic diagram of the experimental program

b. Field spraying test under soybean-maize complex planting pattern

c. Maize collection point arrangement

d. Soybean collection point arrangement

Figure 11 Field spraying test under soybean-maize complex planting pattern

5 Results

5.1 Wind speed data recording and analysis

According to the above test conditions, the airflow velocity at each measuring point in the downwash airflow field of the three downwash airflow field guidance devices is shown in Figure 12, where the horizontal coordinate corresponds to the position of each measurement point in the plane of equal height centered on the Z-axis, and each point of the horizontal coordinate corresponds to the measurement points in Figure 9.

The variation of wind field velocity within the radius of 0.51 m from the center line of the 0.80 m downwash airflow field guidance device at the height of 0.42-0.50 m below the device is presented in Figures 12a and 12b. Within the radius range of 0-0.34 m, the wind velocity of the UAV downwash airflow field decreased with the increase of radius, with the minimum velocity of 0.48 m/s. When the radius exceeded 0.34 m, the wind velocity increased rapidly and reached 3.00 m/s or above.

As shown in Figures 12c-12e, at the height of 0.58-0.66 m below the 0.80 m downwash airflow field guidance device, the wind velocity of the UAV downwash airflow field showed a decreasing trend within the radius range of 0-0.17 m, and increased with the increase of radius when the radius exceeded 0.17 m. Combined with the longitudinal section nephogram of the downwash airflow field guidance device in the previous section, the nozzles of the narrow-width spraying plant protection UAV equipped with the 0.80 m downwash airflow field guidance device were recommended to be arranged at the height of 0-0.50 m below the upper bottom of the guidance device, with a spacing of 0.68 m between the two nozzles. The wind field velocity at the height of 0.42-0.58 m below the 0.92 m downwash airflow field guidance device is presented in Figures 12f-12h. Within the radius range of 0-0.38 m, the wind velocity of the downwash airflow field decreased gradually, with the minimum velocity of 0.13 m/s. When the radius exceeded 0.38 m, the wind velocity increased rapidly and reached 2.90 m/s or above. As shown in Figures 12i and 12j, at the height of 0.66-0.74 m below the 0.92 m downwash airflow field guidance device, the wind velocity of the UAV downwash airflow field showed a decreasing trend within the radius range of 0-0.19 m, and increased with the increase of radius when the radius exceeded 0.19 m, with all wind velocity above 1.00 m/s. Therefore, the nozzles of the narrow-width spraying plant protection UAV equipped with the 0.92 m downwash airflow field guidance device were recommended to be arranged at the height of 0-0.58 m below the upper bottom of the guidance device, with a spacing of 0.76 m between the two nozzles[25].

Figures 12k-12n show the wind field test results of 1.04 m diameter downwash wind field guidance at the height of 0.42-0.66 m below the device, covering the wind speed distribution from the centerline of the guidance device to a radial distance of 0.63 m, with a focus on the radius range of 0-0.42 m. The drone down-pressure wind field velocity decreases with the increase of the radius, and at the lowest point reaches a minimum speed of 0.15 m/s. When the radius exceeds 0.42 m, the wind field velocity rises rapidly, and the wind speed reaches more than 2.50 m/s.

As shown in Figure 12o, at the height of 0.74 m below the 1.04 m downwash airflow field guidance device, the wind velocity of the UAV downwash airflow field showed a decreasing trend within the radius range of 0-0.21 m, and increased with the increase of radius when the radius exceeded 0.21 m, with all wind velocity above 2.70 m/s. Therefore, the nozzles of the narrow-width spraying plant protection UAV equipped with the 1.04 m downwash airflow field guidance device were recommended to be arranged at the height of 0-0.66 m below the upper bottom of the guidance device, with a spacing of 0.84 m between the two nozzles.

5.2 Effective spray width test results and analysis

The collected droplet collection cards were scanned by a scanner, and the droplet density on the cards was measured via DepositScan software[26]. According to the Civil Aviation Industry Standard of the People's Republic of China, "Agricultural Aerial Spraying Operation Quality Technical Indicators", when the airplane carries out ultra-low-volume agricultural spraying operation, the effective spraying width is achieved when the density of droplet coverage of the target reaches more than 15 droplets/cm^2[25]. The droplet density is shown in Figure 13, and the effective spraying widths of the three groups are 1.51 m, 1.42 m, and 1.45 m respectively. Taking the average value, that is to say, the effective spraying width of the UAV is 1.46 m at a flight height of 1.00 m and a speed of 2.50 m/s.

5.3 Analysis of spraying test effects in the field under soybean-maize composite planting pattern

The test cards were collected after the spraying operation, and

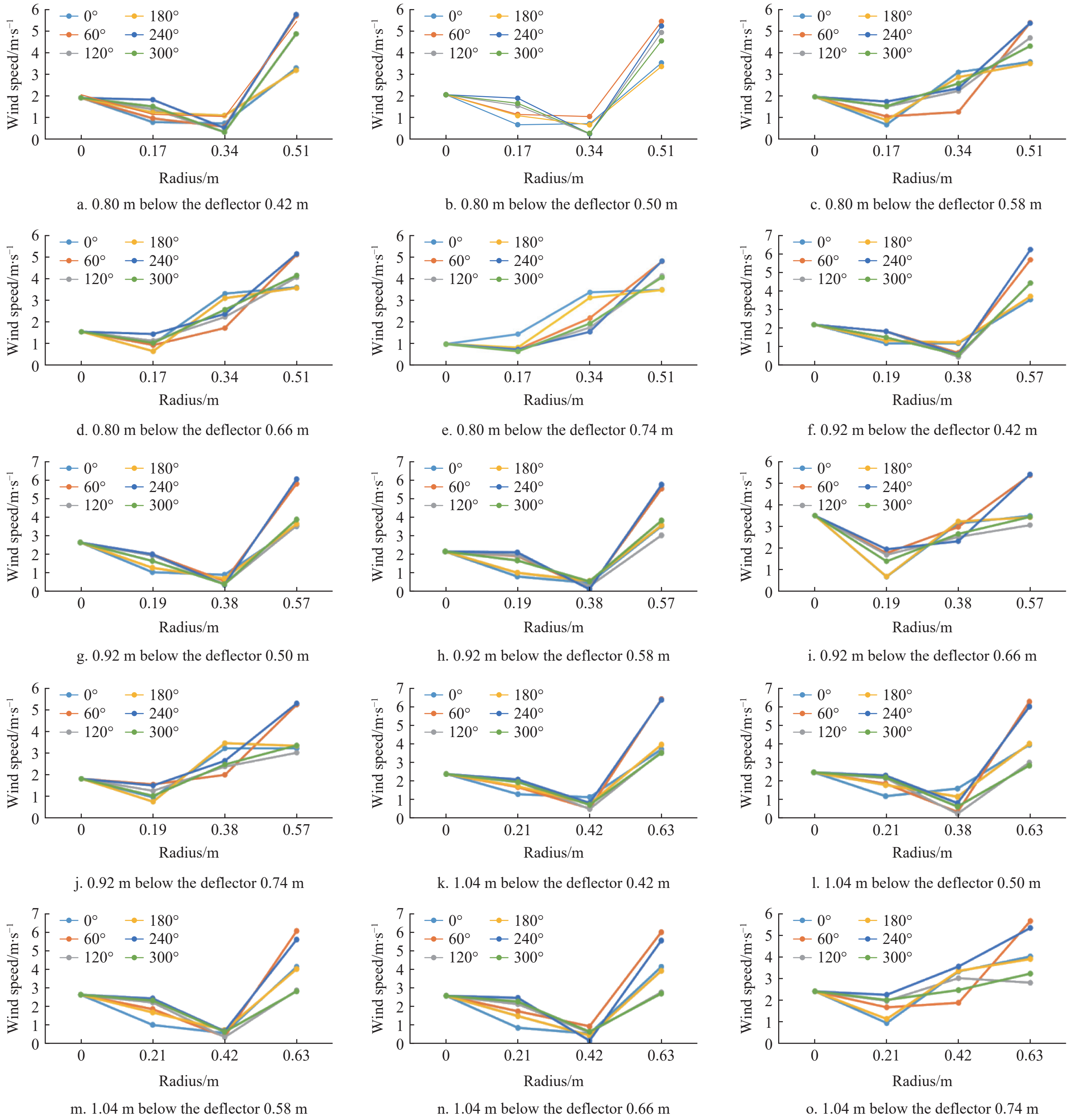

Figure 12 Wind field speed under different deflectors

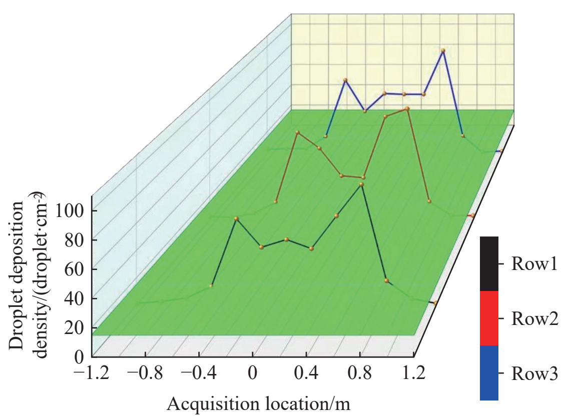

Figure 13 Fog droplet deposition density map

data processing was carried out via image processing method to calculate the deposition rate of each collection point. The results of deposition distribution are listed in Table 1.

It is observed from Table 1 that the droplet deposition was mainly concentrated at the collection points No. 6, 7, and 8, namely the maize canopy area, i.e., at the maize plants. The drift of fog droplets mainly appeared at serial numbers 5 and 9, i.e., at the spacing of maize-soybean belts. The downwash wind field of the UAV was guided to the periphery by the downwash wind field guidance device, and the drifted droplets were rapidly deposited to the ground under the action of the high-speed airflow to prevent droplets from drifting to the soybean plants. The variability of droplet deposition was not obvious in the top, middle, and bottom of the fog droplets.

Table 1 Distribution of droplet deposition

Collection point serial number	Flight vertical distribution								
	Row 1			Row 2			Row 3		
	Upper class	Middle-ranking	Lower strata	Upper class	Middle-ranking	Lower strata	Upper class	Middle-ranking	Lower strata
1	0	0	0	0	0	0	0	0	0
2	0	0	0	0	0	0	0	0	0
3	0	0	0	0	0	0	0	0	0
4	0.040	0.189	0.108	0.012	0.029	0.098	0.001	0.009	0.019
5	0.050	0.212	0.077	0.005	0.082	0.151	0.008	0.089	0.046
6	18.615	16.073	12.317	14.059	15.520	16.711	25.205	31.700	17.210
7	18.697	19.993	15.550	22.483	16.486	17.171	15.718	28.266	31.236
8	17.929	17.640	19.676	20.573	27.292	24.843	21.542	28.203	20.800
9	0.064	0.017	0.054	0.089	0.058	0.053	0.058	0.048	0.033
10	0.099	0.006	0.019	0.056	0.008	0.016	0.011	0.021	0.013
11	0	0	0	0	0	0	0	0	0
12	0	0	0	0	0	0	0	0	0
13	0	0	0	0	0	0	0	0	0

6 Conclusions

1) Based on the CFD method, the simulation of the downwash airflow field of plant protection UAVs equipped with downwash airflow field guidance devices of different sizes was carried out. The simulation of the downwash airflow field of the narrow-width spraying plant protection UAV was completed, and the distribution law of the wind field corresponding to the downwash airflow field guidance devices with different sizes was analyzed. The largest wind speed of the rotor downwash wind field occurs at the center of the rotor, and the further the distance from the rotor, the smaller the speed at the center of the rotor. The downwash airflow field is constrained by the guidance device. Taking the device center as the circle center, the wind speed shows a stepped distribution from the inside to the outside, rising first and then falling. The wind speed of the UAV downwash airflow field was measured via indoor bench tests, and the optimal nozzle installation positions for downwash airflow field guidance devices of different sizes were determined. For the narrow spraying plant protection UAV equipped with guidance devices of 0.80 m, 0.92 m, and 1.04 m in diameter, the optimal nozzle mounting heights are 0-0.50 m, 0-0.58 m, and 0-0.66 m respectively, and the corresponding spacing between adjacent nozzle is 0.68 m, 0.76 m, and 0.84 m.

2) The trial production and test of the multi-rotor plant protection UAV suitable for narrow spraying were completed. Evaluation of the effective spray swath confirmed that the prototype achieves a swath width of 1.46 m when operating at a flight altitude of 1.00 m and a speed of 2.50 m/s, enabling synchronous yet segregated pesticide application for maize and soybean rows. Field trials conducted in a maize–soybean strip intercropping system demonstrated that the downwash airflow guidance device effectively redirects the UAV-induced airflow toward the outer edges of the spray zone. This guidance mechanism promotes rapid droplet deposition onto the ground, thereby significantly reducing drift toward soybean plants. Therefore, the design of the downwash airflow guidance device effectively mitigates droplet drift. By aligning the crop row spacing with the UAV's effective spray swath, this system addresses the challenge of achieving simultaneous and precise pesticide coverage in intercropping systems characterized by varying crop heights and divergent chemical requirements. These improvements reduce pesticide and water consumption, lower production costs, and improve economic benefits. They also support the development of sustainable agricultural practices. Meanwhile, this work provides a novel design strategy for pesticide application equipment suitable for intercropping systems. In future studies, the Beidou differential positioning system can be integrated to realize automatic row-following operation, and crop growth sensors can be adopted to achieve variable-rate spraying, thus promoting the development of intelligent precision pesticide application technology in smart agricultural systems.

Acknowledgements

This research was funded by the Ningxia Key Research and Development Plan Project (Grant No. 2023BCF01051) and the National Key R&D Program of China, Large Load Plant Protection Intelligent UAV Creation and Application (Grant No. 2023 YFD2000200).

[References]

[1] He J S. Application of plant protection drones for pest control in corn-soybean strip compound planting system. Agricultural Engineering Technology, 2024; 44(11): 70–71. (in Chinese)

[2] Zhang T, Dong X, Yin S Z, Yang X J, Yan H R, Gong Q T, et al. Spraying performance of lightweight high clearance boom sprayer in soybean field. Transactions of the CSAM, 2016; 47(S1): 182–188. (in Chinese)

[3] Shang Z Q. Design and experimental study on small electric sprayer for soybean self-propelled striping boom sprayer. Master dissertation. Zhengzhou: Henan Agricultural University, 2021; 97p. (in Chinese)

[4] Wang R, Cao D L, Liu Y S, Jin J M. Design and test of self balancing precise fertilizer and pesticide applying machine. Journal of Agricultural Mechanization Research, 2019; 41(3): 124–129. (in Chinese)

[5] Cheng S S. Design and experimental study of striping boom sprayer for soybean-maize strip intercropping. Master dissertation. Zhengzhou: Henan Agricultural University, 2022; 53p. (in Chinese)

[6] Wang P, Kang Y H, Lee C G, Han X Z, et al. Development of an autonomous drone spraying control system based on the coefficient of variation of spray distribution. Computers and Electronics in Agriculture, 2024; 227: 109529.

[7] Sánchez-Fernández L, Barrera M, Martínez-Guanter J, Pérez-Ruiz M. Drift reduction in orchards through the use of an autonomous UAV system. Computers and Electronics in Agriculture, 2023; 211: 107981.

[8] Shan C F, Xue C, Zhang L C, Song C C, Kaousar R, Wang G B, et al. Effects of different spray parameters of plant protection UAV on the deposition characteristics of droplets in apple trees. Crop Protection, 2024; 184: 106835.

[9] Zhan Y L, Chen P C, Xu W C, Chen S D, Han Y F, Lan Y B, et al. Influence of the downwash airflow distribution characteristics of a plant protection UAV on spray deposit distribution. Biosystems Engineering, 2022; 216: 32–45.

[10] Yang F B, Xue X Y, Cai C, Zhou Q Q. Effect of downwash airflow in hover on droplet motion law for multi-rotor unmanned plant protection machine. Transactions of the CSAE, 2018; 34(2): 64–73. (in Chinese)

[11] Zhang T, Yang X J, Dong X, Liu S M, Wang J J, Dou L J. Experiment on spraying performance of super-high clearance boom sprayer with air-assisted system. Transactions of the CSAM, 2012; 43(10): 66–71. (in Chinese)

[12] Li R F, Han S K, Yang F B. Research on downwash flow and droplet distribution of four-rotor plant protection UAV coupling with wind field. Journal of Chinese Agricultural Mechanization, 2024; 45(7): 81–86. (in Chinese)

[13] Fu Z Z, Guo L Z, Cheng L, Li Q R, Wei Y H. Droplet deposition characteristics and weed control effects of bentazone herbicide sprayed by plant protection drones in oat fields. Acta Agriculturae Universitatis Jiangxiensis, 2024; 46(5): 1221–1232. (in Chinese)

[14] Lan Y B, Shan C F, Wang Q Y, Liu Q, Yang C L, Xie Y J, et al. Effects of different spray additives on droplet deposition characteristics during plant protection UAV spraying operations. Transactions of the CSAE, 2021; 37(16): 31–38. (in Chinese)

[15] Wang G B, Han Y X, Li X, Andaloro J, Chen P C, Hoffmann W C, et al. Field evaluation of spray drift and environmental impact using an agricultural unmanned aerial vehicle (UAV) sprayer. Science of The Total Environment, 2020; 737: 139793.

[16] Zhang H Y, Lan Y B, Wen S, Xu T Y, Yu F H. Research progress in rotor airflow model of plant protection UAV and droplet motion mechanism. Transactions of the CSAE, 2020; 36(22): 1–12. (in Chinese).

[17] Zhang H, Qi L J, Wu Y L, Musiu E M, Cheng Z Z, Wang P. Numerical simulation of airflow field from a six-rotor plant protection drone using lattice Boltzmann method. Biosystems Engineering, 2020; 197: 336–351.

[18] Lei Y, Huang Y, Wang H. Effects of wind disturbance on the aerodynamic performance of a quadrotor MAV during hovering. Sensors, 2021; 2021: 6681716.

[19] Liu Y, Chen B, Zhang J C, Zhang X, Chen X B. Research and development of wind resistance test system for plant protection UAV. Journal of Jiangsu University (Natural Science Edition), 2020; 41(3): 346–352. (in Chinese)

[20] Wang B, Zhang Y, Wang C S, Teng G F. Droplet deposition distribution prediction method for a six-rotor plant protection UAV based on inverse distance weighting. Sensors, 2022; 22(19): 7425.

[21] Wang T, Wen S, Lan Y B, Zhang H Y, Yin X C, Zhang J T. Prediction model for the downwash flow field of single-rotor plant protection UAV using PINNs. Transactions of the CSAE, 2023; 39(6): 83–91. (in Chinese)

[22] Li H Z, Zhu H, Jiang Z H, Lan Y B. Performance characterization on downwash flow and spray drift of multirotor unmanned agricultural aircraft system based on CFD. Int J Agric & Biol Eng, 2022; 15(3): 1–8.

[23] Shi X, Gao S C, Yang D B, Yuan H Z, Yan X J. High-throughput quantification of allura red trace used in determining pesticide deposition utilization by microplate reader. Modern Agrochemicals , 2021; 20(1): 1–7. (in Chinese)

[24] Liu X C, Meng Y H, Zhang Y F, Chen W, Du X T, Hu H Y. An OpenCV-based method for direct detection of droplet deposition parameters on cotton leaves. China Cotton, 2024; 51(10): 9–14. (in Chinese)

[25] Xie Y J, Wang G B, Wang B J, Shan C F, Lan Y B. Selection of nozzle type and parameter optimization in herbicide spraying process of plant protection UAV. Journal of Chinese Agricultural Mechanization, 2021; 42(4): 61–69. (in Chinese).

[26] Ma K, Zhang Z Y, Dong X Y, Qiu B J. Design and test of a portable droplet deposition detection system. Journal of Agricultural Mechanization Research, 2023; 45(5): 49–54. (in Chinese)